
Tailoring Mixup to Data for Calibration

Quentin Bouniot, Pavlo Mozharovskiy & Florence d'Alché-Buc
LTCI, Télécom Paris, Institut Polytechnique de Paris, France
name.surname@telecom-paris.fr

Abstract

Among all data augmentation techniques proposed so far, linear interpolation of training samples, also called *Mixup*, has found to be effective for a large panel of applications. Along with improved performance, Mixup is also a good technique for improving calibration and predictive uncertainty. However, mixing data carelessly can lead to manifold intrusion, i.e., conflicts between the synthetic labels assigned and the true label distributions, which can deteriorate calibration. In this work, we argue that the likelihood of manifold intrusion increases with the distance between data to mix. To this end, we propose to dynamically change the underlying distributions of interpolation coefficients depending on the similarity between samples to mix, and define a flexible framework to do so without losing in diversity. We provide extensive experiments for classification and regression tasks, showing that our proposed method improves performance and calibration of models, while being much more efficient. The code for our work is available at https://github.com/qbouniot/sim_kernel_mixup.

1 Introduction

The *Vicinal Risk Minimization (VRM)* principle (Chapelle et al., 2000) improves on the well-known *Empirical Risk Minimization (ERM)* (Vapnik, 1998) for training deep neural networks by drawing virtual samples from a vicinity around true training data. This data augmentation principle is known to improve the generalization ability of deep neural networks when the number of observed data is small compared to the task complexity. In practice, the method of choice to implement it relies on hand-crafted procedures to mimic natural perturbations (Yaeger et al., 1996; Ha and Bunke, 1997; Simard et al., 2002). However, one counterintuitive but effective and less application-specific approach for generating synthetic data is through interpolation, or mixing, of two or more training data.

The process of interpolating between data have been discussed multiple times before (Chawla et al., 2002; Wang et al., 2017; Inoue, 2018; Tokozume et al., 2018), but *Mixup* (Zhang et al., 2018) represents the most popular implementation and continues to be studied in recent works (Pinto et al., 2022; Liu et al., 2022b; Wang et al., 2023). Ever since its introduction, it has been a widely studied data augmentation technique spanning applications to *image classification and generation* (Zhang et al., 2018), *semantic segmentation* (Franchi et al., 2021; Islam et al., 2023), *natural language processing* (Verma et al., 2019), *speech processing* (Meng et al., 2021), *time series and tabular regression* (Yao et al., 2022b) or *geometric deep learning* (Kan et al., 2023), to that extent of being now an integral component of competitive state-of-the-art training settings (Wightman et al., 2021). The idea behind *Mixup* can be seen as an efficient approximation of *VRM*, by using a linear interpolation of data points selected from within the same batch to reduce computation overheads (Zhang et al., 2018).

The process of Mixup as a data augmentation during training can be roughly separated in three phases: (i) selecting tuples (most often pairs) of points to mix together, (ii) sampling coefficients that will govern the interpolation to generate synthetic points, (iii) applying a specific interpolation

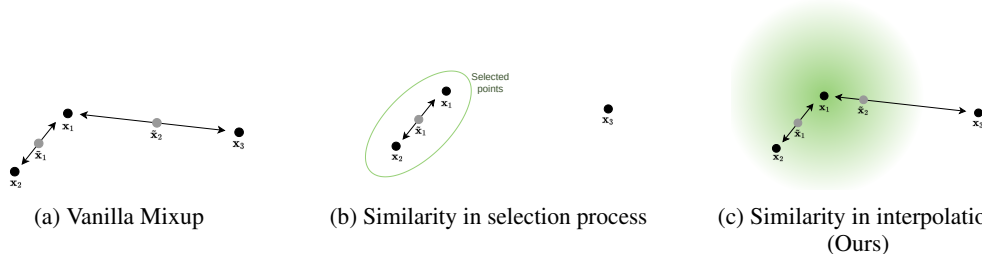


Figure 1: Different approaches to take into account similarity between points in Mixup. (*Left*) Vanilla Mixup process, any pair of points can be mixed with the same interpolation. (*Middle*) Only similar pairs are mixed. (*Right*) Interpolation is governed by similarity.

procedure between the points weighted by the coefficients sampled. Methods in the literature have mainly focused on the first and third phases, *i.e.*, the process of sampling points to mix through predefined criteria (Hwang et al., 2022; Yao et al., 2022b,a; Palakkadavath et al., 2022; Teney et al., 2023) and on the interpolation itself, by applying sophisticated and application-specific functions (Yun et al., 2019; Franchi et al., 2021; Venkataramanan et al., 2022; Kan et al., 2023). On the other hand, these *interpolation coefficients*, when they exist, are always sampled from the same distribution throughout training. Recent works have shown that mixing carelessly different points can result in incorrect labels and hurt generalization (Guo et al., 2019; Yao et al., 2022b; Liu et al., 2023), while mixing similar points helps in diversity (Chawla et al., 2002; Dablain et al., 2022). Furthermore, several previous work have highlighted a trade-off between performance and calibration in Mixup (Thulasidasan et al., 2019; Pinto et al., 2022; Wang et al., 2023).

In this work, we aim to provide an *efficient* and *flexible* framework for taking similarity into account when interpolating points. Notably, we argue that similarity should influence the *interpolation coefficients* rather than the selection process of points to mix, to avoid losing in diversity. A high similarity should result in strong interpolation, while a low similarity should lead to almost no changes. Consequently, controlling the interpolation through the distance of the points to mix should improve calibration by reducing *manifold intrusion* and *label noise*. Figure 1 illustrates the difference between taking into account similarity in the selection process and through the interpolation. Selecting only similar pairs to mix restricts the possible synthetic data generated (*Middle*). Governing interpolation coefficients through similarity of points avoid restricting possible directions of mixing (*Right*). Furthermore, restricting the mixing operation by the distance between points forces the synthetic samples to be more likely in the vicinity of original samples, making the overall process closer to VRM. Our contributions towards this goal are as follows:

- We show that taking into account similarity when mixing can alleviate label noise and improve calibration. Mixing only similar data leads to better calibration than including dissimilar ones.
- We present a flexible framework to dynamically change the distributions of interpolation coefficients. We apply a **similarity kernel** that takes into account the distance between points to select a parameter for the distribution tailored to each pair to mix. The underlying distribution of interpolation is warped to be stronger for similar points and weaker otherwise.
- We quantitatively ascertain the effectiveness of our **Similarity Kernel Mixup** with extensive experiments on multiple datasets, from image classification to regression tasks, and multiple deep neural network architectures. Our approach achieves a better trade-off between improving *accuracy* and *calibration*. Additionally, we highlight the **efficiency** of our method, obtaining competitive results with less computation per iteration, and reaching the best performance globally faster.

2 Related Work

2.1 Data augmentation based on mixing data

The idea of mixing two or more training data points to generate additional synthetic ones has been developed in various ways in the literature.

Non-linear interpolation Non-linear combinations are mainly studied for dealing with image data. Instead of a naive linear interpolation between two images, the augmentation process is done using more complex non-linear functions, such as cropping, patching and pasting images together (Takahashi et al., 2019; Summers and Dinneen, 2019; Yun et al., 2019; Kim et al., 2020) or through subnetworks (Ramé et al., 2021; Liu et al., 2022b; Venkataramanan et al., 2022). Not only are these non-linear operations focused on images, but they generally introduce a significant computational overhead compared to the simpler linear one (Zhu et al., 2020; Li et al., 2022). The recent *R-Mixup* (Kan et al., 2023), on the other hand, considers other Riemannian geodesics rather than the Euclidean straight line for graphs, but is also computationally expensive.

Linear interpolation Mixing samples online through linear interpolation represents the most efficient and general technique compared to the ones presented above (Zhang et al., 2018; Inoue, 2018; Tokozume et al., 2018). Among these different approaches, combining data from the same batch also avoids additional samplings. Several follow-up works extend Mixup from different perspectives. *Manifold Mixup* (Verma et al., 2019) interpolates data in the feature space, *k-Mixup* (Greenewald et al., 2021) extends the interpolation to use k points instead of a pair, *Remix* (Chou et al., 2020) separates the interpolation in the label space and the input space. Notably, *AdaMixUp* (Guo et al., 2019) learns to predict a mixing policy to apply to avoid manifold intrusion using two additional parallel models with intrusion losses. This leads to a more complex training and includes more parameters to learn. Furthermore, the predicted range is very narrow around 0.5, reducing diversity of the mixed samples, and the training includes non-mixed samples, making the approach similar to the recent *Regmixup* (Pinto et al., 2022). *Local Mixup* (Baena et al., 2022) is another approach interested on the manifold intrusion problem, by weighting the loss function with the distance between the points using K-nearest neighbors graphs. However, this results in completely discarding the interpolation with points that are far away, losing potential augmentation directions and, therefore, in diversity. Moreover, these two methods are focusing on improving generalization, while we are looking at the problem of manifold intrusion through the lens of improving *calibration*.

Selecting points A recent family of methods applies an online linear combination on specifically selected pairs of examples (Yao et al., 2022b,a; Hwang et al., 2022; Palakkadavath et al., 2022; Teney et al., 2023), across classes (Yao et al., 2022a) or across domains (Yao et al., 2022a; Palakkadavath et al., 2022; Tian et al., 2023). These methods achieve impressive results on distribution shift and out-of-distribution generalization (Yao et al., 2022a), but recent theoretical developments have shown that much of the improvements are linked to a resampling effect from the restrictions in the selection process, and are unrelated to the mixing operation (Teney et al., 2023). These selective criteria also induce high computational overhead. One related approach is *C-Mixup* (Yao et al., 2022b), that fits a Gaussian kernel on the labels distance between points in regression tasks. Then points to mix together are sampled from the full training set according to the learned Gaussian density. However, the Gaussian kernel is computed on all the data before training, which is difficult when there is a lot of data and no explicit distance between them.

2.2 Calibration in classification and regression

Calibration is a metric to quantify uncertainty, measuring the difference between a model’s confidence in its predictions and the actual probability of those predictions being correct. We refer the reader to Appendix C for a short review of calibration metrics

In classification Modern deep neural network for image classification are now known to be *overconfident* leading to *miscalibration* (Guo et al., 2017). One can rely on *temperature scaling* (Guo et al., 2017) to improve calibration *post-hoc*, or using different techniques during learning such as *ensembling* (Lakshminarayanan et al., 2017; Wen et al., 2021; Laurent et al., 2022), *explicit penalties* (Pereyra et al., 2017; Kumar et al., 2018; Moon et al., 2020; Cheng and Vasconcelos, 2022), or *implicit* ones (Müller et al., 2019; Lin et al., 2017; Mukhoti et al., 2020; Liu et al., 2022a), including notably through *mixup* (Thulasidasan et al., 2019; Pinto et al., 2022; Noh et al., 2023). One should note that calibration results should be compared after temperature scaling, since it can change the ordering of results (Ashukha et al., 2020).

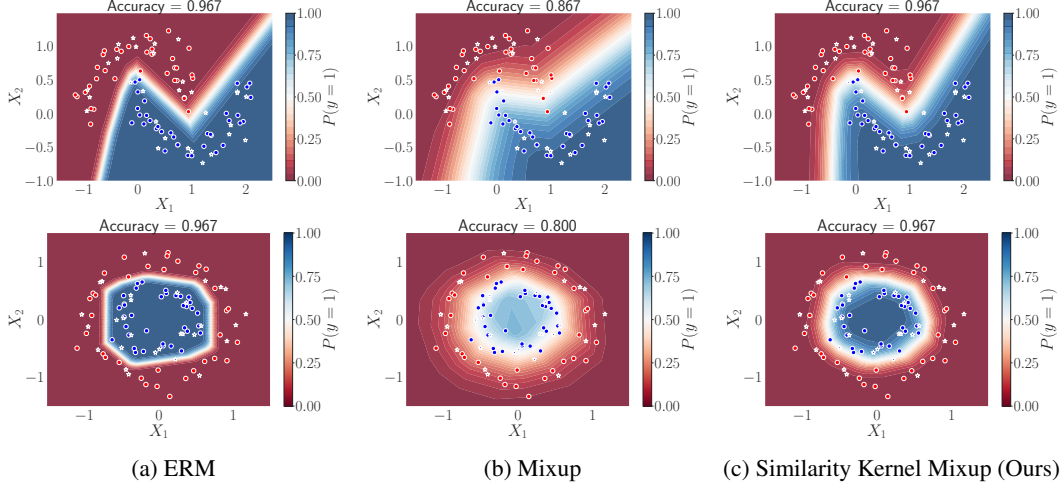


Figure 2: Decision frontiers and data used during training (*circles*) and testing (*stars*) for (a) ERM, (b) Mixup, and (c) our Similarity Kernel Mixup, on Moons (*top*) and Circles (*bottom*) toy datasets.

Calibration-driven Mixup methods The problem of the trade-off between performance and calibration with Mixup has been extensively studied in previous works (Thulasidasan et al., 2019; Zhang et al., 2022; Pinto et al., 2022; Wang et al., 2023). Notably, Wang et al. (2023) observed that calibration using Mixup can be degraded after temperature scaling. Therefore, they proposed another improvement of mixup, *MIT* (Wang et al., 2023), by generating two sets of mixed samples and then deriving their correct label. *RegMixup* (Pinto et al., 2022) considers Mixup as a regularization term, using stronger interpolation on every pair. Finally, *RankMixup* (Noh et al., 2023) uses the interpolation coefficients from multiple mixed pairs as an additional supervisory signal for ranking of confidence. We propose a more efficient method to achieve a good trade-off between accuracy and calibration with Mixup.

In regression The problem of calibration in deep learning has also been studied for regression tasks (Kuleshov et al., 2018; Song et al., 2019; Laves et al., 2020; Levi et al., 2022), where it is more complex as we lack a simple measure of predictive confidence. In this case, regression models are usually evaluated under the variational inference framework with Monte Carlo (MC) Dropout (Gal and Ghahramani, 2016) to quantify confidence.

In our work, we use a *similarity kernel* to mix more strongly similar data and avoid mixing less similar ones, leading to preserving label quality and confidence of the network. As opposed to all other methods discussed above, we also show the flexibility of our approach by its effectiveness on both classification and regression tasks. We detail our framework, the similarity used and the intuition behind below.

3 Similarity Kernel Mixup

Preliminary notations and background First, we define the notations and elaborate on the learning conditions that will be considered throughout the paper. Let $\mathcal{D} = \{(\mathbf{x}_i, y_i)\}_{i=1}^N = (\mathbf{X}, \mathbf{y}) \in \mathbb{X}^N \times \mathbb{Y}^N \subset \mathbb{R}^{d \times N} \times \mathbb{R}^N$ be the training dataset. We want to learn a *model* f_θ parameterized by $\theta \in \Theta \subset \mathbb{R}^p$, that predicts $\hat{y} := f_\theta(\mathbf{x})$ for any $\mathbf{x} \in \mathbb{X}$. For classification tasks, we have $\mathbb{Y} \subset \mathbb{R}^c$, and we further assume that the model f_θ can be separated into an encoder part h_φ and classification weights $\mathbf{w} \in \mathbb{R}^c$, such that $\forall \mathbf{x} \in \mathbb{X}, f_\theta(\mathbf{x}) = \mathbf{w}^\top h_\varphi(\mathbf{x})$. To learn our model, we optimize the *weights* of the model θ in a stochastic manner, by repeating the minimization process of the empirical risk computed on *batch* of data $\mathcal{B}_t = \{(\mathbf{x}_i, y_i)\}_{i=1}^n$ sampled from the training set, for $t \in \{1, \dots, T\}$ iterations.

With *Mixup* (Zhang et al., 2018), at each iteration t , the empirical risk is computed on augmented batch of data $\tilde{\mathcal{B}}_t = \{(\tilde{\mathbf{x}}_i, \tilde{y}_i)\}_{i=1}^n$, such that $\tilde{\mathbf{x}}_i := \lambda_t \mathbf{x}_i + (1 - \lambda_t) \mathbf{x}_{\sigma_t(i)}$ and $\tilde{y}_i := \lambda_t y_i + (1 - \lambda_t) y_{\sigma_t(i)}$, with $\lambda_t \sim \text{Beta}(\alpha, \alpha)$ and $\sigma_t \in \mathfrak{S}_n$ a random permutation of n elements sampled uniformly. Thus, each input is mixed with another input randomly selected from the same batch, and λ_t represents

the strength of the interpolation between them. Besides simplicity, mixing elements within the batch significantly reduces both memory and computation costs.

In the following parts, we introduce a more general extension of this framework using warping functions, that spans different variants of *Mixup*, while preserving its efficiency. First, we discuss and illustrate the *manifold intrusion problem* with *Mixup* and its impact.

3.1 Manifold Intrusion

The assumption underlying our work is that there exists a trade-off in data augmentation procedures between adding diversity and introducing uncertainty. In *mixup*, uncertainty can be introduced through manifold intrusion (Guo et al., 2019), *i.e.*, conflicts between the synthetic labels of the mixed-up examples and the labels of original training data. More specifically, we argue that in *mixup* the likelihood of conflict in the synthetic label increases with the distance between the two points. As data live in manifolds of the representation space, the linear combination of two points far from each other can lie in a different manifold than the linear combination of the labels. The further away the points are, the more manifolds can exist in between. We illustrate this problem on the *Moons* and *Circles* toy problems in Figure 2. We observe that a model with *Mixup* (*middle*) can lead to worst confidence and performance compared to standard ERM (*left*), due to manifold intrusion. Since the moons are intertwined and non-convex, linear interpolations from the same moon can lie in the other (*top*). Likewise, interpolations of data from the external circle can fall into the inner one (*bottom*). Using our Similarity Kernel Mixup approach (*right*) described in this paper, we recover the accuracy and achieve more meaningful confidence scores.

Then, we conduct an empirical analysis on real datasets that compares accuracy and calibration metrics using the classic *ERM*, the original *Mixup*, and a *modified version of Mixup* that selects pairs to mix according to a given quantile of the overall pairwise distances within the batch. To have equivalent proportions of possible data to mix with (*same diversity*), we analyze results when mixing only pairs of points with distances lower than a given quantile q , and higher than the quantile $q' = 1 - q$. More specifically, we show in Figure 3 the results for $q = 0.75$ of the overall pairwise distances within the batch, using a Resnet34 (He et al., 2016) on CIFAR10 and CIFAR100 (Krizhevsky et al., 2009) datasets. Detailed values for this experiment with different quantiles q can be found in Appendix D, and implementation details in Section 4. First, we observe that *Mixup* improves upon ERM’s accuracy, but can degrade calibration depending on the dataset, which is consistent with findings from Wang et al. (2023). Then, when selecting pairs according to distance, a sufficiently high proportion of data to mix is necessary to preserve accuracy ($q > 0.5$). Finally, mixing data with lower distances achieves a better calibration as opposed to mixing data with higher distances.

These results show that there is a trade-off between adding diversity by increasing the proportion of elements to mix, and uncertainty by mixing elements far from each other. Furthermore, it shows that we cannot restrict pairs to mix by selecting data solely based on distance, as it can degrade performance by reducing diversity of synthetic samples. To better control this trade-off with *Mixup*, we propose to tailor *interpolation coefficients* to the training data, from the distance between the points to mix. We detail our framework in the next part.

3.2 Warped Mixup

To dynamically change the interpolation depending on the similarity between points, we rely on *warping functions* ω_τ , to *warp* interpolation coefficients λ_t at every iteration t depending on the parameter τ . These functions ω_τ are *bijective transformations* from $[0, 1]$ to $[0, 1]$ defined as such:

$$\omega_\tau(\lambda_t) = I_{\lambda_t}^{-1}(\tau, \tau) \quad \text{with} \quad I_{\lambda_t} = \int_0^{\lambda_t} \frac{u^{\tau-1}(1-u)^{\tau-1}}{B(\tau, \tau)} du, \quad (1)$$

where I_{λ_t} is the *regularized incomplete beta function*, which is the *cumulative distribution function* (CDF) of the Beta distribution, $B(\tau, \tau)$ is a normalization constant and $\tau \in \mathbb{R}_+^*$ is the *warping parameter* that governs the strength and direction of the warping. Similar warping has been used in the *Bayesian Optimization* literature (Snoek et al., 2014), however many other suitable bijection with sigmoidal shape could be considered in our case. Our motivation behind such ω_τ is to preserve the same type of distribution after warping, *i.e.*, Beta distributions with symmetry around 0.5, through *Inverse Transform Sampling* (see Appendix F for the proof):

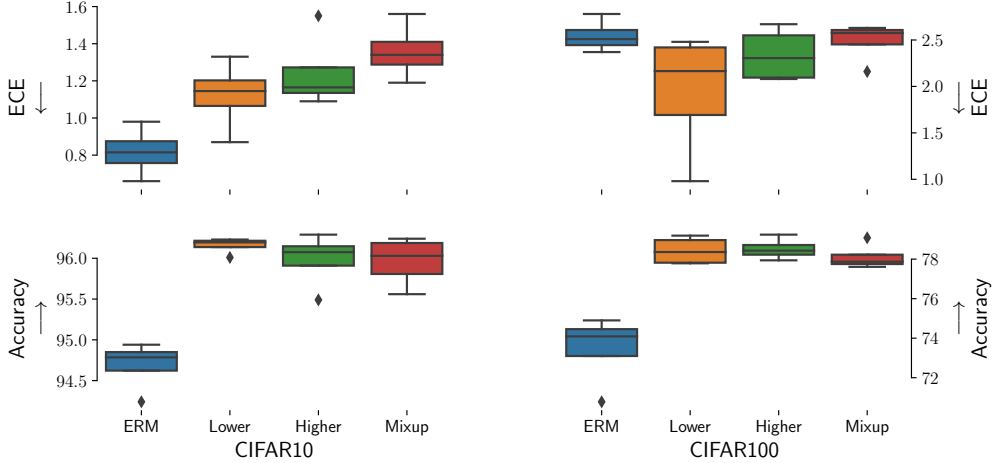


Figure 3: Performance (Accuracy in %, *higher is better*, **bottom**) and calibration (ECE, *lower is better*, **top**) after Temperature Scaling (TS) Guo et al. (2017) comparison with Resnet34 on CIFAR10 (**left**) and CIFAR100 (**right**) datasets. We compare results when mixing only elements with distance **Higher** (in *green*) than the 0.25 quantile, and **Lower** (in *orange*) than the 0.75 quantile of all pairwise distances within each batch.

Proposition 3.1. *Let $\lambda \sim \mathcal{U}([0, 1])$. Then $\omega_\tau(\lambda) \sim \text{Beta}(\tau, \tau)$ for any $\tau > 0$.*

One should note that according to Proposition 3.1, the initial interpolation parameter λ should follow a *uniform distribution* for $\omega_\tau(\lambda)$ to follow a $\text{Beta}(\tau, \tau)$ distribution. Thus, in the remaining of the paper, we always draw λ according to a uniform distribution (or equivalently, a $\text{Beta}(1, 1)$), which has the additional benefit of *removing α as a hyperparameter*. Figure 4a illustrates the shape of ω_τ and their behavior with respect to τ . These functions have a symmetric behavior around $\tau = 1$ (in *blue*), for which warped outputs remain unchanged. When $\tau > 1$ (in *red and purple*) they are pulled towards the center (0.5), and when $\tau < 1$ (in *orange and green*), they are pushed towards the extremes (0 and 1). We thus extend the Mixup framework with warping:

$$\lambda_t \sim \text{Beta}(1, 1), \quad \begin{aligned} \tilde{\mathbf{x}}_i &:= \omega_\tau(\lambda_t)\mathbf{x}_i + (1 - \omega_\tau(\lambda_t))\mathbf{x}_{\sigma_t(i)} \\ \tilde{y}_i &:= \omega_\tau(\lambda_t)y_i + (1 - \omega_\tau(\lambda_t))y_{\sigma_t(i)}. \end{aligned} \quad (2)$$

In addition to providing a general framework, using warping functions proves to be more computationally efficient, which we discuss in details in Appendix G. In the following part, we present our method to select the right τ depending on the data to mix, to dynamically change the distribution of the interpolation coefficients.

3.3 Similarity Kernel

Recall that our main goal is to apply stronger interpolation between similar points, and reduce interpolation otherwise. Since the behavior of Beta distributions and ω_τ are logarithmic with respect to τ , therefore, the parameter τ should be exponentially correlated with the distance, with a symmetric behavior around 1. To this end, we define a class of *similarity kernels*, based on a normalized and centered Gaussian kernel, that outputs the correct warping parameter for the given pair of points. Given a batch of data $\mathbf{x} = \{\mathbf{x}_i\}_{i=1}^n \in \mathbb{R}^{d \times n}$, the index of the first element in the mix $i \in \{1, \dots, n\}$, along with the permutation $\sigma \in \mathfrak{S}_n$ to obtain the index of the second element, we compute the following *similarity kernel*:

$$\tau(\mathbf{x}, i, \sigma; \tau_{\max}, \tau_{\text{std}}) = \tau_{\max} \exp\left(-\frac{\bar{d}_n(\mathbf{x}_i, \mathbf{x}_{\sigma(i)}) - 1}{2\tau_{\text{std}}^2}\right), \quad (3)$$

$$\text{with } \bar{d}_n(\mathbf{x}_i, \mathbf{x}_{\sigma(i)}) = \frac{\|\mathbf{x}_i - \mathbf{x}_{\sigma(i)}\|_2^2}{\frac{1}{n} \sum_{j=1}^n \|\mathbf{x}_j - \mathbf{x}_{\sigma(j)}\|_2^2}, \quad (4)$$

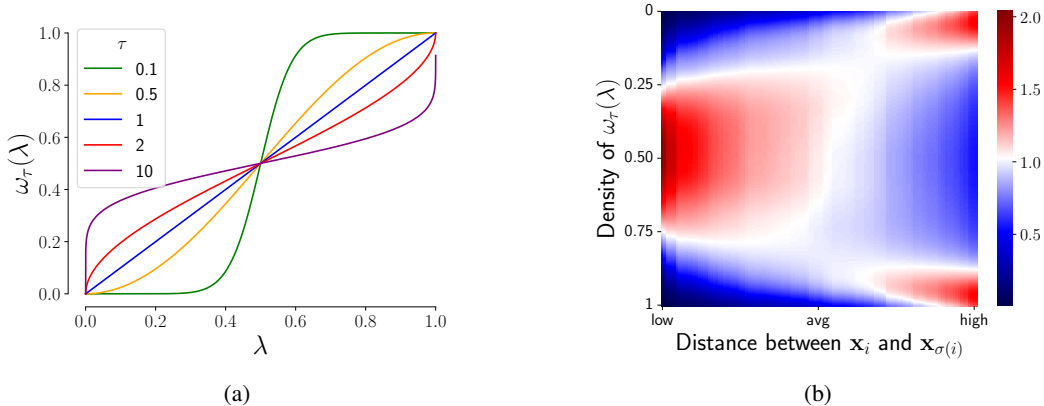


Figure 4: **(a)** Behavior of ω_τ for different values of τ . **(b)** Density of interpolation coefficients $\omega_\tau(\lambda)$ after warping with the similarity kernel depending on the distance between pairs.

where \bar{d}_n is the squared L_2 distance rescaled by the mean distance over the batch, and τ_{\max} , τ_{std} are respectively the *amplitude* and *standard deviation (std)* of the Gaussian, which are hyperparameters of the similarity kernel. The amplitude τ_{\max} governs the strength of the interpolation in average, and τ_{std} the extent of mixing. In practice, we found that these two parameters could be tuned separately, and that choosing a good τ_{std} is more important than τ_{\max} . The framework presented allows to measure similarity between points in any space that can represent them. More specifically, for classification tasks, we use the L_2 distance between embeddings, *i.e.*, $\bar{d}_n(h_\varphi(\mathbf{x}_i), h_\varphi(\mathbf{x}_{\sigma(i)}))$, while for regression tasks, we use the distance between labels, *i.e.*, $\bar{d}_n(y_i, y_{\sigma(i)})$, following Yao et al. (2022b).

Our motivation behind this kernel is to have $\tau > 1$ when the two points to mix are similar, *i.e.*, the distance is lower than average, to increase the mixing effect, and $\tau < 1$ otherwise, to reduce the mixing. Figure 4b illustrates the evolution of the density of *warped* interpolation coefficients $\omega_\tau(\lambda)$, depending on the distance between the points to mix. Close distances (*left part of the heatmap*) induce strong interpolations, while far distances (*right part of the heatmap*) reduce interpolation. Using this similarity kernel to find the correct τ to parameterize the *Beta distribution* defines our full *Similarity Kernel (SK) Mixup* framework. A detailed algorithm of the training procedure can be found in Appendix E, and an in-depth discussion about warping and similarity measures in Appendix J.

4 Experiments

4.1 Protocols

Image Classification We follow experimental settings from previous works (Liu et al., 2022a; Wang et al., 2023; Noh et al., 2023) and evaluate our approach on CIFAR-10, CIFAR-100 (Krizhevsky et al., 2009), Tiny-Imagenet (Deng et al., 2009) and Imagenet (Russakovsky et al., 2015) datasets, using Resnet34, Resnet50 and Resnet101 architectures (He et al., 2016). We evaluate calibration using ECE and AECE (Naeini et al., 2015; Guo et al., 2017), negative log likelihood (NLL) (Hastie et al., 2009) and Brier score (Brier, 1950), after finding the optimal temperature on the validation set through Temperature Scaling (Guo et al., 2017). Results are reproduced and averaged over 4 different random runs, and we report standard deviation between the runs.

Regression Here again, we follow settings of previous work on regression (Yao et al., 2022b). We evaluate performance on Airfoil (Kooperberg, 1997), Exchange-Rate and Electricity (Lai et al., 2018) datasets using Mean Averaged Percentage Error (MAPE), along with Uncertainty Calibration Error (UCE) (Laves et al., 2020) and Expected Normalized Calibration Error (ENCE) (Levi et al., 2022) for calibration. Results are reproduced and averaged over 10 different random runs. We also report standard deviation between the runs.

A presentation of the different calibration metrics used can be found in Appendix C, along with a detailed description of implementation settings and hyperparameters in Appendix H.

Table 1: Comparison of Performance (Accuracy in %) and calibration (ECE, Brier, NLL) *after Temperature Scaling* with Resnet34 on CIFAR10 and CIFAR100. Best in **bold**, second best underlined.

Methods	α	τ_{std}	CIFAR10				CIFAR100			
			Accuracy (\uparrow)	ECE (\downarrow)	Brier (\downarrow)	NLL (\downarrow)	Accuracy (\uparrow)	ECE (\downarrow)	Brier (\downarrow)	NLL (\downarrow)
ERM	-	-	94.69 \pm 0.27	0.82 \pm 0.11	8.07 \pm 0.31	17.50 \pm 0.61	73.47 \pm 1.59	2.54 \pm 0.15	36.47 \pm 2.05	100.82 \pm 6.93
Mixup	1	-	95.97 \pm 0.27	1.36 \pm 0.13	6.53 \pm 0.36	16.35 \pm 0.72	78.11 \pm 0.57	2.49 \pm 0.19	31.06 \pm 0.69	87.94 \pm 1.98
	0.5	-	95.71 \pm 0.26	1.33 \pm 0.08	7.03 \pm 0.46	17.47 \pm 1.18	77.14 \pm 0.67	2.7 \pm 0.36	32.01 \pm 0.93	91.22 \pm 3.05
	0.1	-	95.37 \pm 0.22	1.13 \pm 0.11	7.37 \pm 0.36	17.43 \pm 0.79	76.01 \pm 0.62	2.54 \pm 0.24	33.41 \pm 0.57	93.96 \pm 1.76
Mixup IO	1	-	95.16 \pm 0.22	0.6 \pm 0.11	7.3 \pm 0.33	15.56 \pm 0.67	74.44 \pm 0.49	2.02 \pm 0.14	35.25 \pm 0.43	96.5 \pm 1.62
	0.5	-	95.31 \pm 0.17	0.58 \pm 0.06	7.12 \pm 0.21	15.09 \pm 0.45	74.45 \pm 0.6	1.94 \pm 0.09	35.2 \pm 0.58	96.75 \pm 1.89
	0.1	-	95.12 \pm 0.21	0.7 \pm 0.09	7.38 \pm 0.27	15.76 \pm 0.55	74.21 \pm 0.46	2.39 \pm 0.11	35.38 \pm 0.48	98.24 \pm 1.81
SK Mixup (Ours)	0.2	-	96.29 \pm 0.07	1.35 \pm 0.14	6.37 \pm 0.11	15.97 \pm 0.22	78.13 \pm 0.52	1.31 \pm 0.23	31.18 \pm 0.72	85.38 \pm 1.92
	0.4	-	96.42 \pm 0.24	0.53 \pm 0.06	6.02 \pm 0.41	15.28 \pm 0.92	78.86 \pm 0.83	1.42 \pm 0.19	30.1 \pm 1.17	84.22 \pm 3.35
	0.6	-	96.36 \pm 0.09	0.52 \pm 0.08	6.12 \pm 0.09	15.7 \pm 0.29	78.63 \pm 0.27	1.74 \pm 0.30	30.41 \pm 0.30	84.97 \pm 1.12
	0.8	-	96.00 \pm 0.41	0.56 \pm 0.05	6.63 \pm 0.58	16.64 \pm 1.27	79.12 \pm 0.52	1.66 \pm 0.16	29.75 \pm 0.57	82.82 \pm 1.62
	1.0	-	96.25 \pm 0.07	0.55 \pm 0.12	6.31 \pm 0.18	16.14 \pm 0.55	78.51 \pm 0.94	1.49 \pm 0.03	30.46 \pm 1.04	85.06 \pm 3.18

Table 2: Comparison of performance (Accuracy in %) and calibration (ECE, AECE) *after Temperature Scaling*, with Resnet101 on CIFAR10, CIFAR100 and Tiny-Imagenet datasets. \dagger : Results reported from Noh et al. (2023). Best in **bold**, second best underlined, for reported results and ours separately.

Methods	Acc. (\uparrow)	CIFAR10		Acc. (\uparrow)	CIFAR100		Acc. (\uparrow)	Tiny-Imagenet	
		ECE (\downarrow)	AECE (\downarrow)		ECE (\downarrow)	AECE (\downarrow)		ECE (\downarrow)	AECE (\downarrow)
ERM \dagger	94.46	<u>0.92</u>	<u>0.85</u>	77.48	2.63	2.66	66.04	3.50	3.52
MMCE \dagger	94.99	1.15	12.9	<u>77.82</u>	3.06	2.80	66.44	3.40	3.38
ECP \dagger	93.97	1.72	1.70	76.81	2.92	3.04	66.20	2.72	2.70
LS \dagger	94.18	1.51	3.10	76.91	4.38	4.55	65.52	2.51	2.72
FL \dagger	93.59	1.12	1.37	76.12	2.58	2.51	64.02	2.18	2.09
Mixup \dagger	95.50	1.18	2.33	78.74	3.69	3.65	66.41	1.97	1.95
FLSD \dagger	93.26	0.93	0.94	76.61	2.04	1.78	64.02	1.85	1.81
CRL \dagger	95.04	1.12	2.03	77.60	3.32	3.31	65.87	<u>1.60</u>	1.52
CPC \dagger	<u>95.36</u>	1.52	2.37	77.50	2.96	3.23	66.44	3.93	3.74
MbLS \dagger	95.13	1.38	3.25	77.45	5.49	6.52	65.81	1.62	1.68
RegMixup \dagger	95.03	<u>0.92</u>	0.94	76.93	<u>1.36</u>	1.92	63.26	1.86	1.68
RankMixup \dagger	94.25	0.65	0.56	76.46	1.10	1.40	64.89	1.57	1.94
ERM	93.97 \pm 0.03	0.58 \pm 0.01	0.63 \pm 0.01	77.99 \pm 0.31	2.16 \pm 0.25	2.10 \pm 0.27	65.7 \pm 0.07	1.62 \pm 0.19	1.57 \pm 0.2
Mixup	94.78 \pm 0.13	1.47 \pm 0.01	2.59 \pm 0.02	77.50 \pm 0.18	2.58 \pm 0.01	2.67 \pm 0.20	67.80 \pm 0.54	1.93 \pm 0.02	1.68 \pm 0.01
Manifold Mixup	94.75 \pm 0.03	1.57 \pm 0.05	2.61 \pm 0.03	77.76 \pm 1.35	3.07 \pm 0.22	3.16 \pm 0.17	68.57 \pm 0.04	2.11 \pm 0.01	2.06 \pm 0.01
RankMixup	94.42 \pm 0.17	0.70 \pm 0.11	0.63 \pm 0.14	77.27 \pm 0.08	2.12 \pm 0.20	2.04 \pm 0.19	65.40 \pm 0.01	1.48 \pm 0.02	1.44 \pm 0.06
MIT-A	95.27 \pm 0.01	0.93 \pm 0.01	1.59 \pm 0.13	77.23 \pm 0.56	2.39 \pm 0.03	2.32 \pm 0.05	68.03 \pm 0.09	1.52 \pm 0.15	1.57 \pm 0.05
SK Mixup (Ours)	<u>95.04 \pm 0.07</u>	0.47 \pm 0.01	0.98 \pm 0.05	78.20 \pm 0.46	1.11 \pm 0.06	1.38 \pm 0.11	67.60 \pm 0.01	1.06 \pm 0.01	1.19 \pm 0.02

4.2 Classification

Throughout our experiments in classification, we use by default $\tau_{max} = 1$ (unless stated otherwise), since we found that *the impact on calibration was mainly controlled by τ_{std}* , as discussed below.

Effect of τ_{std} We present in Table 1 the performance and calibration results on CIFAR10 and CIFAR100 with a Resnet34, to study the effect of varying τ_{std} . We compare the results with *Mixup* (Zhang et al., 2018) and *Mixup-IO* (Wang et al., 2023), which mixes between Inputs Only while keeping one-hot labels, for varying values of α . These two versions of Mixup show the trade-off between the effect of confidence penalty (in Mixup) that can hurt calibration on the one hand, and trivial confidence promotion (in Mixup-IO) that can hurt accuracy on the other hand. By varying only τ_{std} , therefore changing the *extent* of mixing, we can achieve a better and finer trade-off between these two effects, and *improving both calibration and accuracy*. Furthermore, it shows that our Similarity Kernel Mixup method obtains better results than simply changing α in Mixup and Mixup-IO. For other experiments, we first performed cross-validation to select τ_{std} . In general, we found that $\tau_{std} = 0.25$ worked for all datasets. We refer the reader to Appendix I for more details on cross-validation.

Comparison with state of the art In Table 2, we present an extensive comparison of results on CIFAR10, CIFAR100 and Tiny-ImageNet with a Resnet101, and on Imagenet for Resnet50 in Table 3. We compare performance and calibration results reported *in the same settings* for various approaches from Noh et al. (2023), including *implicit methods* such as LS (Müller et al., 2019), FL (Lin et al., 2017), FLSD (Mukhoti et al., 2020), MbLS (Liu et al., 2022a), Mixup (Thulasidasan et al., 2019) and RegMixup (Pinto et al., 2022), and *explicit methods*, such as ECP (Pereyra et al., 2017), MMCE (Kumar et al., 2018), CRL (Moon et al., 2020), CPC (Cheng and Vasconcelos, 2022).

Table 3: Comparison of performance (Accuracy in %) and calibration (ECE, AECE), with Resnet50 on Imagenet dataset. Best in **bold**, second best underlined.

Methods	Acc. (\uparrow)	ECE (\downarrow)	AECE (\downarrow)
ERM	76.06 \pm 0.35	4.12 \pm 0.22	4.05 \pm 0.20
Mixup	76.59 \pm 0.5	1.8 \pm 0.21	1.77 \pm 0.19
Manifold Mixup	<u>76.61 \pm 0.27</u>	<u>1.77 \pm 0.15</u>	<u>1.77 \pm 0.18</u>
RankMixup	<u>76.33 \pm 0.06</u>	<u>2.07 \pm 0.16</u>	<u>2.1 \pm 0.14</u>
MIT-A	76.7 \pm 0.29	1.8 \pm 0.08	1.74 \pm 0.1
Similarity Kernel Mixup (<i>Ours</i>)	76.2 \pm 0.26	1.46 \pm 0.09	1.4 \pm 0.07

Table 4: Performance (RMSE, MAPE) and calibration (UCE, ENCE) comparison on regression tasks. Best in **bold**, second best underlined.

Methods	Airfoil			Exchange Rate			Electricity		
	MAPE (\downarrow)	UCE (\downarrow)	ENCE (\downarrow)	MAPE (\downarrow)	UCE (\downarrow)	ENCE (\downarrow)	MAPE (\downarrow)	UCE (\downarrow)	ENCE (\downarrow)
ERM	1.720 \pm 0.219	107.6 \pm 19.2	2.10% \pm 0.78	1.924 \pm 0.287	0.82% \pm 0.28	3.64% \pm 0.74	15.263 \pm 0.383	0.76% \pm 0.08	22.07% \pm 1.27
Mixup	2.003 \pm 0.126	147.1 \pm 34.0	2.12% \pm 0.63	1.926 \pm 0.284	0.74% \pm 0.22	<u>3.52% \pm 0.59</u>	14.944 \pm 0.386	0.62% \pm 0.07	24.28% \pm 2.47
Manifold Mixup	1.964 \pm 0.111	126.0 \pm 15.8	2.06% \pm 0.64	2.006 \pm 0.346	0.86% \pm 0.29	3.82% \pm 0.85	14.872 \pm 0.409	0.69% \pm 0.05	24.53% \pm 1.44
RegMixup	1.725 \pm 0.092	<u>105.0 \pm 23.1</u>	1.92% \pm 0.73	1.918 \pm 0.290	0.80% \pm 0.24	3.66% \pm 0.73	<u>14.790 \pm 0.395</u>	0.66% \pm 0.12	23.68% \pm 2.53
C-Mixup	1.706 \pm 0.104	111.2 \pm 32.6	1.90% \pm 0.75	<u>1.893 \pm 0.222</u>	0.78% \pm 0.20	3.60% \pm 0.64	15.085 \pm 0.533	0.69% \pm 0.11	23.54% \pm 1.90
SK Mixup (<i>Ours</i>)	1.609 \pm 0.137	93.8 \pm 25.5	1.85% \pm 0.84	1.814 \pm 0.241	0.76% \pm 0.21	3.40% \pm 0.56	14.649 \pm 0.191	0.61% \pm 0.05	23.93% \pm 2.05

We have also reproduced results of Mixup, Manifold Mixup (Verma et al., 2019), RankMixup (Noh et al., 2023) and MIT-A (Wang et al., 2023) in the same settings on multiple random seeds, using official codes and hyperparameters provided by the authors. We can see from these results that we achieve competitive performance for accuracy and improves calibration compared to other *Calibration-driven Mixup methods*. Notably, our approach always improves accuracy over ERM.

4.3 Regression

To demonstrate the flexibility of our framework regarding different tasks, we provide experiments on regression for tabular data and time series. Regression tasks have the advantage of having an obvious meaningful distance between points, which is distance between labels. Therefore, following Yao et al. (2022b), we directly measure the similarity between two points by the *distance between their labels*, i.e., $\bar{d}_n(y_i, y_{\sigma(i)})$. This avoids the computation of distance on embeddings and makes our method *as fast as the original Mixup*. In Table 4, we compare our Kernel Warping Mixup with Mixup (Zhang et al., 2018), Manifold Mixup (Verma et al., 2019), RegMixup (Pinto et al., 2022), and C-Mixup

Table 5: Efficiency comparison between Mixup methods. We report the number of batch of data in memory at each iteration, the best epoch measured on validation data, time per epoch (in seconds) and total training time to reach the best epoch (in seconds).

(a) Image classification on CIFAR10, CIFAR100 and Tiny-imagenet datasets, with a Resnet50.

Method	Batch in memory	CIFAR10			CIFAR100			Tiny-Imagenet		
		Best Epoch	Time	Total Time	Best Epoch	Time	Total Time	Best Epoch	Time	Total Time
RankMixup	4	147	78	11485	177	78	13806	80	540	43380
MIT-A	2	189	46	8694	167	46	7659	82	305	24908
SK Mixup	1	183	28	5138	160	28	4480	69	189	13104

(b) Time series regression on Electricity dataset.

Methods	Batch in memory	Best Epoch	Time	Total Time
C-Mixup	2	87	46.51	4046
RegMixup	2	85	11.46	975
SK Mixup (<i>Ours</i>)	1	78	11.16	867

(Yao et al., 2022b). We can see that our approach achieves competitive results with state-of-the-art C-Mixup, in both performance (MAPE) and calibration metrics.

4.4 Efficiency Comparison

Our method achieves competitive results while being *much more efficient* than other state-of-the-art approaches. Indeed, as can be seen in Table 5, our Similarity Kernel Mixup is about $1.5\times$ faster than MIT-A, about $3\times$ faster than RankMixup, and about $4\times$ faster than C-Mixup.

Additionally, we use *a single batch of data* for each iteration, while MIT-A requires training on *twice* the amount of data per batch, and *four times* the amount of data per batch for RankMixup. This adds significant memory constraints which limits the maximum batch size possible in practice. Unlike C-Mixup, our approach does not rely on *sampling rates* calculated before training, which add a lot of computational overhead and are difficult to obtain for large datasets.

5 Conclusion

Motivated by calibration in both classification and regression tasks, we present *Similarity Kernel Mixup*, a flexible framework for linearly interpolating data during training, based on a *similarity kernel*. The coefficients governing the interpolation are warped to change their underlying distribution depending on the similarity between the points to mix, such that similar data are mixed more strongly than less similar ones, preserving calibration by avoiding *manifold intrusion and label noise*. This provides a *more efficient* data augmentation approach than *Calibration-driven Mixup methods*, both in terms of time and memory, with a better trade-off between performance and calibration improvement. We show through extensive experiments the effectiveness of the approach in classification as well as in regression. It is also worth noting that the proposed framework could be extended to other Mixup variants such as CutMix (Yun et al., 2019) or Manifold Mixup (Verma et al., 2019). Future works include applications to more complex tasks such as semantic segmentation or depth estimation.

References

- Ashukha, A., Lyzhov, A., Molchanov, D., and Vetrov, D. (2020). Pitfalls of in-domain uncertainty estimation and ensembling in deep learning. In *International Conference on Learning Representations*.
- Baena, R., Drumetz, L., and Gripon, V. (2022). A local mixup to prevent manifold intrusion. In *30th European Signal Processing Conference, EUSIPCO 2022, Belgrade, Serbia, August 29 - Sept. 2, 2022*, pages 1372–1376. IEEE.
- Brier, G. W. (1950). Verification of forecasts expressed in terms of probability. *Monthly weather review*, 78(1):1–3.
- Chapelle, O., Weston, J., Bottou, L., and Vapnik, V. (2000). Vicinal risk minimization. In Leen, T. K., Dietterich, T. G., and Tresp, V., editors, *Advances in Neural Information Processing Systems 13*, pages 416–422. MIT Press.
- Chawla, N. V., Bowyer, K. W., Hall, L. O., and Kegelmeyer, W. P. (2002). Smote: synthetic minority over-sampling technique. *Journal of artificial intelligence research*, 16:321–357.
- Cheng, J. and Vasconcelos, N. (2022). Calibrating deep neural networks by pairwise constraints. In *Proceedings of the IEEE/CVF Conference on Computer Vision and Pattern Recognition*, pages 13709–13718.
- Chou, H., Chang, S., Pan, J., Wei, W., and Juan, D. (2020). Remix: Rebalanced mixup. In Bartoli, A. and Fusiello, A., editors, *Computer Vision - ECCV 2020 Workshops - Glasgow, UK, August 23-28, 2020, Proceedings, Part VI*, volume 12540 of *Lecture Notes in Computer Science*, pages 95–110. Springer.
- Dablain, D., Krawczyk, B., and Chawla, N. V. (2022). Deepsmote: Fusing deep learning and smote for imbalanced data. *IEEE Transactions on Neural Networks and Learning Systems*.

- Deng, J., Dong, W., Socher, R., Li, L.-J., Li, K., and Fei-Fei, L. (2009). Imagenet: A large-scale hierarchical image database. In *2009 IEEE conference on computer vision and pattern recognition*, pages 248–255. Ieee.
- Franchi, G., Belkhir, N., Ha, M. L., Hu, Y., Bursuc, A., Blanz, V., and Yao, A. (2021). Robust semantic segmentation with superpixel-mix. In *32nd British Machine Vision Conference 2021, BMVC 2021, Online, November 22-25, 2021*, page 158. BMVA Press.
- Gal, Y. and Ghahramani, Z. (2016). Dropout as a Bayesian approximation: Representing model uncertainty in deep learning. In *Proceedings of the 33rd International Conference on Machine Learning (ICML-16)*.
- Greenewald, K. H., Gu, A., Yurochkin, M., Solomon, J., and Chien, E. (2021). k-mixup regularization for deep learning via optimal transport. *CoRR*, abs/2106.02933.
- Guo, C., Pleiss, G., Sun, Y., and Weinberger, K. Q. (2017). On calibration of modern neural networks. In *International conference on machine learning*. PMLR.
- Guo, H., Mao, Y., and Zhang, R. (2019). Mixup as locally linear out-of-manifold regularization. In *Proceedings of the AAAI conference on artificial intelligence*, volume 33, pages 3714–3722.
- Ha, T. M. and Bunke, H. (1997). Off-line, handwritten numeral recognition by perturbation method. *IEEE Trans. Pattern Anal. Mach. Intell.*, 19(5):535–539.
- Hastie, T., Tibshirani, R., Friedman, J. H., and Friedman, J. H. (2009). *The elements of statistical learning: data mining, inference, and prediction*, volume 2. Springer.
- He, K., Zhang, X., Ren, S., and Sun, J. (2016). Deep residual learning for image recognition. In *2016 IEEE Conference on Computer Vision and Pattern Recognition, CVPR 2016, Las Vegas, NV, USA, June 27-30, 2016*, pages 770–778. IEEE Computer Society.
- Hwang, I., Lee, S., Kwak, Y., Oh, S. J., Teney, D., Kim, J.-H., and Zhang, B.-T. (2022). Selecmix: Debaised learning by contradicting-pair sampling. *Advances in Neural Information Processing Systems*, 35:14345–14357.
- Inoue, H. (2018). Data augmentation by pairing samples for images classification. *arXiv preprint arXiv:1801.02929*.
- Islam, M. A., Kowal, M., Derpanis, K. G., and Bruce, N. D. (2023). Segmix: Co-occurrence driven mixup for semantic segmentation and adversarial robustness. *International Journal of Computer Vision*, 131(3):701–716.
- Kan, X., Li, Z., Cui, H., Yu, Y., Xu, R., Yu, S., Zhang, Z., Guo, Y., and Yang, C. (2023). R-mixup: Riemannian mixup for biological networks. In Singh, A., Sun, Y., Akoglu, L., Gunopulos, D., Yan, X., Kumar, R., Ozcan, F., and Ye, J., editors, *Proceedings of the 29th ACM SIGKDD Conference on Knowledge Discovery and Data Mining, KDD 2023, Long Beach, CA, USA, August 6-10, 2023*, pages 1073–1085. ACM.
- Kim, J., Choo, W., and Song, H. O. (2020). Puzzle mix: Exploiting saliency and local statistics for optimal mixup. In *Proceedings of the 37th International Conference on Machine Learning, ICML 2020, 13-18 July 2020, Virtual Event*, volume 119 of *Proceedings of Machine Learning Research*, pages 5275–5285. PMLR.
- Kingma, D. P. and Ba, J. (2014). Adam: A method for stochastic optimization. *arXiv preprint arXiv:1412.6980*.
- Kooperberg, C. (1997). Statlib: an archive for statistical software, datasets, and information. *The American Statistician*, 51(1):98.
- Krizhevsky, A., Hinton, G., et al. (2009). Learning multiple layers of features from tiny images.
- Kuleshov, V., Fenner, N., and Ermon, S. (2018). Accurate uncertainties for deep learning using calibrated regression. In *International conference on machine learning*, pages 2796–2804. PMLR.

- Kumar, A., Sarawagi, S., and Jain, U. (2018). Trainable calibration measures for neural networks from kernel mean embeddings. In *International Conference on Machine Learning*, pages 2805–2814. PMLR.
- Lai, G., Chang, W.-C., Yang, Y., and Liu, H. (2018). Modeling long-and short-term temporal patterns with deep neural networks. In *The 41st international ACM SIGIR conference on research & development in information retrieval*, pages 95–104.
- Lakshminarayanan, B., Pritzel, A., and Blundell, C. (2017). Simple and scalable predictive uncertainty estimation using deep ensembles. *Advances in neural information processing systems*, 30.
- Laurent, O., Lafage, A., Tartaglione, E., Daniel, G., Martinez, J.-m., Bursuc, A., and Franchi, G. (2022). Packed ensembles for efficient uncertainty estimation. In *The Eleventh International Conference on Learning Representations*.
- Laves, M.-H., Ihler, S., Fast, J. F., Kahrs, L. A., and Ortmaier, T. (2020). Well-calibrated regression uncertainty in medical imaging with deep learning. In *Medical Imaging with Deep Learning*, pages 393–412. PMLR.
- Levi, D., Gispan, L., Giladi, N., and Fetaya, E. (2022). Evaluating and calibrating uncertainty prediction in regression tasks. *Sensors*, 22(15):5540.
- Li, S., Wang, Z., Liu, Z., Wu, D., and Li, S. Z. (2022). Openmixup: Open mixup toolbox and benchmark for visual representation learning. *CoRR*, abs/2209.04851.
- Lin, T.-Y., Goyal, P., Girshick, R., He, K., and Dollár, P. (2017). Focal loss for dense object detection. In *Proceedings of the IEEE international conference on computer vision*, pages 2980–2988.
- Liu, B., Ben Ayed, I., Galdran, A., and Dolz, J. (2022a). The devil is in the margin: Margin-based label smoothing for network calibration. In *Proceedings of the IEEE/CVF Conference on Computer Vision and Pattern Recognition*, pages 80–88.
- Liu, Z., Li, S., Wu, D., Liu, Z., Chen, Z., Wu, L., and Li, S. Z. (2022b). Automix: Unveiling the power of mixup for stronger classifiers. In Avidan, S., Brostow, G. J., Cissé, M., Farinella, G. M., and Hassner, T., editors, *Computer Vision - ECCV 2022: 17th European Conference, Tel Aviv, Israel, October 23-27, 2022, Proceedings, Part XXIV*, volume 13684 of *Lecture Notes in Computer Science*, pages 441–458. Springer.
- Liu, Z., Wang, Z., Guo, H., and Mao, Y. (2023). Over-training with mixup may hurt generalization. In *The Eleventh International Conference on Learning Representations*.
- Meng, L., Xu, J., Tan, X., Wang, J., Qin, T., and Xu, B. (2021). Mixspeech: Data augmentation for low-resource automatic speech recognition. In *ICASSP 2021-2021 IEEE International Conference on Acoustics, Speech and Signal Processing (ICASSP)*, pages 7008–7012. IEEE.
- Moon, J., Kim, J., Shin, Y., and Hwang, S. (2020). Confidence-aware learning for deep neural networks. In *Proceedings of the 37th International Conference on Machine Learning*, pages 7034–7044. PMLR.
- Mukhoti, J., Kulharia, V., Sanyal, A., Golodetz, S., Torr, P., and Dokania, P. (2020). Calibrating deep neural networks using focal loss. *Advances in Neural Information Processing Systems*, 33:15288–15299.
- Müller, R., Kornblith, S., and Hinton, G. E. (2019). When does label smoothing help? *Advances in neural information processing systems*, 32.
- Naeini, M. P., Cooper, G., and Hauskrecht, M. (2015). Obtaining well calibrated probabilities using bayesian binning. In *Proceedings of the AAAI conference on artificial intelligence*, volume 29.
- Noh, J., Park, H., Lee, J., and Ham, B. (2023). Rankmixup: Ranking-based mixup training for network calibration. In *Proceedings of the IEEE/CVF International Conference on Computer Vision*, pages 1358–1368.

- Palakkadavath, R., Nguyen-Tang, T., Gupta, S., and Venkatesh, S. (2022). Improving domain generalization with interpolation robustness. In *NeurIPS 2022 Workshop on Distribution Shifts: Connecting Methods and Applications*.
- Pereyra, G., Tucker, G., Chorowski, J., Kaiser, Ł., and Hinton, G. (2017). Regularizing neural networks by penalizing confident output distributions. *arXiv preprint arXiv:1701.06548*.
- Pinto, F., Yang, H., Lim, S.-N., Torr, P., and Dokania, P. K. (2022). Regmixup: Mixup as a regularizer can surprisingly improve accuracy and out distribution robustness. In *Advances in Neural Information Processing Systems*.
- Ramé, A., Sun, R., and Cord, M. (2021). Mixmo: Mixing multiple inputs for multiple outputs via deep subnetworks. In *2021 IEEE/CVF International Conference on Computer Vision, ICCV 2021, Montreal, QC, Canada, October 10-17, 2021*, pages 803–813. IEEE.
- Russakovsky, O., Deng, J., Su, H., Krause, J., Satheesh, S., Ma, S., Huang, Z., Karpathy, A., Khosla, A., Bernstein, M. S., Berg, A. C., and Fei-Fei, L. (2015). Imagenet large scale visual recognition challenge. *Int. J. Comput. Vis.*, 115(3):211–252.
- Simard, P. Y., LeCun, Y. A., Denker, J. S., and Victorri, B. (2002). Transformation invariance in pattern recognition—tangent distance and tangent propagation. In *Neural networks: tricks of the trade*, pages 239–274. Springer.
- Snoek, J., Swersky, K., Zemel, R., and Adams, R. (2014). Input warping for bayesian optimization of non-stationary functions. In *International Conference on Machine Learning*, pages 1674–1682. PMLR.
- Song, H., Diethe, T., Kull, M., and Flach, P. (2019). Distribution calibration for regression. In *International Conference on Machine Learning*, pages 5897–5906. PMLR.
- Srivastava, N., Hinton, G., Krizhevsky, A., Sutskever, I., and Salakhutdinov, R. (2014). Dropout: a simple way to prevent neural networks from overfitting. *The journal of machine learning research*, 15(1):1929–1958.
- Summers, C. and Dinneen, M. J. (2019). Improved mixed-example data augmentation. In *2019 IEEE winter conference on applications of computer vision (WACV)*, pages 1262–1270. IEEE.
- Takahashi, R., Matsubara, T., and Uehara, K. (2019). Data augmentation using random image cropping and patching for deep cnns. *IEEE Transactions on Circuits and Systems for Video Technology*, 30(9):2917–2931.
- Teney, D., Wang, J., and Abbasnejad, E. (2023). Selective mixup helps with distribution shifts, but not (only) because of mixup. *arXiv preprint arXiv:2305.16817*.
- Thulasidasan, S., Chennupati, G., Bilmes, J. A., Bhattacharya, T., and Michalak, S. (2019). On mixup training: Improved calibration and predictive uncertainty for deep neural networks. *Advances in Neural Information Processing Systems*, 32.
- Tian, H., Liu, B., Zhu, T., Zhou, W., and Philip, S. Y. (2023). Cifair: Constructing continuous domains of invariant features for image fair classifications. *Knowledge-Based Systems*, 268:110417.
- Tokozume, Y., Ushiku, Y., and Harada, T. (2018). Between-class learning for image classification. In *Proceedings of the IEEE conference on computer vision and pattern recognition*, pages 5486–5494.
- Vapnik, V. (1998). *Statistical learning theory*. Wiley.
- Venkataramanan, S., Kijak, E., Amsaleg, L., and Avrithis, Y. (2022). AlignMixup: Improving representations by interpolating aligned features. In *2022 IEEE/CVF Conference on Computer Vision and Pattern Recognition (CVPR)*, pages 19152–19161. IEEE.
- Verma, V., Lamb, A., Beckham, C., Najafi, A., Mitliagkas, I., Lopez-Paz, D., and Bengio, Y. (2019). Manifold mixup: Better representations by interpolating hidden states. In Chaudhuri, K. and Salakhutdinov, R., editors, *Proceedings of the 36th International Conference on Machine Learning*, volume 97 of *Proceedings of Machine Learning Research*, pages 6438–6447. PMLR.

- Wang, D.-B., Li, L., Zhao, P., Heng, P.-A., and Zhang, M.-L. (2023). On the pitfall of mixup for uncertainty calibration. In *Proceedings of the IEEE/CVF Conference on Computer Vision and Pattern Recognition*, pages 7609–7618.
- Wang, J., Perez, L., et al. (2017). The effectiveness of data augmentation in image classification using deep learning. *Convolutional Neural Networks Vis. Recognit*, 11(2017):1–8.
- Wen, Y., Jerfel, G., Muller, R., Dusenberry, M. W., Snoek, J., Lakshminarayanan, B., and Tran, D. (2021). Combining ensembles and data augmentation can harm your calibration. In *International Conference on Learning Representations*.
- Wightman, R., Touvron, H., and Jegou, H. (2021). Resnet strikes back: An improved training procedure in timm. In *NeurIPS 2021 Workshop on ImageNet: Past, Present, and Future*.
- Yaeger, L., Lyon, R., and Webb, B. (1996). Effective training of a neural network character classifier for word recognition. In Mozer, M., Jordan, M., and Petsche, T., editors, *Advances in Neural Information Processing Systems*, volume 9. MIT Press.
- Yao, H., Wang, Y., Li, S., Zhang, L., Liang, W., Zou, J., and Finn, C. (2022a). Improving out-of-distribution robustness via selective augmentation. In *International Conference on Machine Learning*, pages 25407–25437. PMLR.
- Yao, H., Wang, Y., Zhang, L., Zou, J. Y., and Finn, C. (2022b). C-mixup: Improving generalization in regression. *Advances in Neural Information Processing Systems*, 35:3361–3376.
- Yun, S., Han, D., Chun, S., Oh, S. J., Yoo, Y., and Choe, J. (2019). Cutmix: Regularization strategy to train strong classifiers with localizable features. In *2019 IEEE/CVF International Conference on Computer Vision, ICCV 2019, Seoul, Korea (South), October 27 - November 2, 2019*, pages 6022–6031. IEEE.
- Zhang, H., Cisse, M., Dauphin, Y. N., and Lopez-Paz, D. (2018). mixup: Beyond empirical risk minimization. In *International Conference on Learning Representations*.
- Zhang, L., Deng, Z., Kawaguchi, K., and Zou, J. (2022). When and how mixup improves calibration. In *International Conference on Machine Learning*, pages 26135–26160. PMLR.
- Zhu, J., Shi, L., Yan, J., and Zha, H. (2020). Automix: Mixup networks for sample interpolation via cooperative barycenter learning. In *Computer Vision—ECCV 2020: 16th European Conference, Glasgow, UK, August 23–28, 2020, Proceedings, Part X 16*, pages 633–649. Springer.

A Broader Impact

This paper presents work whose goal is to improve the calibration of machine learning models. Calibration is the process of improving the reliability of the confidence score associated with predictions. This is an important step towards the development of trustworthy models. Having better calibrated models can also help in the detection of biases, overfitting or out-of-distribution data, which can prevent models from being misused in practice.

B Limitations

The majority of theoretical analysis around mixup have been focused on generalization, while we are interested on calibration. Analyzing the impact on calibration is very difficult, as we also need to take into account the effect of Temperature Scaling (TS) Guo et al. (2017) on a validation set. Indeed, TS can change ordering of results Ashukha et al. (2020), and, more importantly, Wang et al. (2023) observed that calibration using Mixup can be worse than ERM after TS. This is an observation that we also confirm in our experiments (e.g. in Table 1). Thus, an analysis including temperature scaling would be required first for vanilla Mixup before analyzing our proposed method. This would be a significant contribution on its own, and our future works include to explore this direction.

Our approach also introduces two additional hyperparameters. However, since in our case we always draw initial parameters λ from $\text{Beta}(1, 1)$, α is not a hyperparameter anymore. Then, τ_{max} and τ_{std}

can be tuned separately, and, as mentioned in Section 4.2, we found that impact on calibration was mainly controlled by τ_{std} . Furthermore, one should note that we always used $\tau_{std} = 0.25$ in image classification experiments, showing our approach is not sensitive to hyperparameter choice between datasets. We discuss selection of hyperparameters with cross-validation in Appendix I.

C Introduction to Calibration Metrics

As discussed in Section 2.2, calibration measures the difference between predictive confidence and actual probability. More formally, with \hat{y} and $y \in \mathbb{Y}$, respectively the model’s prediction and target label, and \hat{p} its predicted confidence, a perfectly calibrated model should satisfy $P(\hat{y} = y | \hat{p} = p) = p$, for $p \in [0, 1]$.

We use several metrics for calibration in the paper, namely, ECE, AECE, Brier score and NLL for classification tasks, and UCE and ENCE for regression tasks. We formally introduce all of them here.

C.1 Metrics for classification tasks

NLL The *negative log-likelihood* (NLL) is a common metric for a model’s prediction quality (Hastie et al., 2009). It is equivalent to cross-entropy in multi-class classification. NLL is defined as:

$$\text{NLL}(\mathbf{x}, \mathbf{y}) = -\frac{1}{N} \sum_{i=1}^N \log(\hat{p}(\mathbf{y}_i | \mathbf{x}_i)), \quad (5)$$

where $\hat{p}(\mathbf{y}_i | \mathbf{x}_i)$ represents the confidence of the model in the output associated to \mathbf{x}_i for the target class \mathbf{y}_i .

Brier score The Brier score (Brier, 1950) for multi-class classification is defined as

$$\text{Brier}(\mathbf{x}, \mathbf{y}) = -\frac{1}{N} \sum_{i=1}^N \sum_{j=1}^c (\hat{p}(y_{(i,j)} | \mathbf{x}_i) - y_{(i,j)})^2, \quad (6)$$

where we assume that the target label \mathbf{y}_i is represented as a one-hot vector over the c possible class, *i.e.*, $\mathbf{y}_i \in \mathbb{R}^c$. Brier score is the mean square error (MSE) between predicted confidence and target.

ECE Expected Calibration Error (ECE) is a popular metric for calibration performance for classification tasks in practice. It approximates the difference between accuracy and confidence in expectation by first grouping all the samples into M equally spaced bins $\{B_m\}_{m=1}^M$ with respect to their confidence scores, then taking a weighted average of the difference between accuracy and confidence for each bin. Formally, ECE is defined as (Guo et al., 2017):

$$\text{ECE} := \sum_{m=1}^M \frac{|B_m|}{N} |\text{acc}(B_m) - \text{conf}(B_m)|, \quad (7)$$

with $\text{acc}(B_m) = \frac{1}{|B_m|} \sum_{i \in B_m} \mathbb{1}_{\hat{y}_i = y_i}$ the accuracy of bin B_m , and $\text{conf}(B_m) = \frac{1}{|B_m|} \sum_{i \in B_m} \hat{p}(\mathbf{y}_i | \mathbf{x}_i)$ the average confidence within bin B_m .

AECE The Adaptive ECE (AECE) is computed similarly to ECE, with the difference that bin sizes are calculated to evenly distribute samples across the bins.

C.2 Metrics for regression tasks

A probabilistic regression model takes $\mathbf{x} \in \mathbb{X}$ as input and outputs a mean $\mu_y(\mathbf{x})$ and a variance $\sigma_y^2(\mathbf{x})$ targeting the ground-truth $y \in \mathbb{Y}$. The UCE and ENCE calibration metrics are both extension of ECE for regression tasks to evaluate *variance calibration*. They both apply a binning scheme with M bins over the predicted variance.

Table 6: Performance (Accuracy in %) and calibration (ECE, Brier, NLL) *before and after Temperature Scaling (TS)* Guo et al. (2017) with Resnet34 when mixing only elements higher or lower than a quantile q . Best in **bold**, second best underlined.

Dataset	Quantile of Distance	Accuracy (\uparrow)	ECE (\downarrow)	Brier (\downarrow)	NLL (\downarrow)	TS ECE (\downarrow)	TS Brier (\downarrow)	TS NLL (\downarrow)	
C10	Lower 0.0 / Higher 1.0 (ERM)	94.69 \pm 0.27	3.65 \pm 0.22	8.90 \pm 0.4	24.57 \pm 1.04	0.82 \pm 0.11	8.07 \pm 0.31	17.50 \pm 0.61	
	Lower 1.0 / Higher 0.0 (Mixup)	95.97 \pm 0.27	12.3 \pm 0.92	8.54 \pm 0.64	25.68 \pm 1.53	1.36 \pm 0.13	6.53 \pm 0.36	16.35 \pm 0.72	
	Lower 0.1	95.70 \pm 0.24	1.58 \pm 0.3	7.12 \pm 0.36	17.9 \pm 1.01	0.99 \pm 0.3	7.08 \pm 0.37	16.1 \pm 0.85	
	Lower 0.25	95.73 \pm 0.18	<u>2.42 \pm 0.55</u>	7.12 \pm 0.25	19.54 \pm 1.1	1.74 \pm 0.45	7.07 \pm 0.26	19.39 \pm 1.11	
	Lower 0.5	95.88 \pm 0.28	3.04 \pm 0.4	6.67 \pm 0.34	16.68 \pm 0.84	1.56 \pm 0.28	6.68 \pm 0.34	15.86 \pm 0.71	
	Lower 0.75	96.16 \pm 0.09	3.63 \pm 0.32	6.33 \pm 0.14	16.55 \pm 0.59	1.12 \pm 0.16	6.35 \pm 0.15	<u>15.20 \pm 0.44</u>	
	Lower 0.9	96.31 \pm 0.08	3.71 \pm 0.34	<u>6.20 \pm 0.24</u>	<u>16.65 \pm 0.41</u>	1.10 \pm 0.05	6.14 \pm 0.11	15.16 \pm 0.29	
	Higher 0.9	95.58 \pm 0.34	2.72 \pm 0.2	7.39 \pm 0.49	20.54 \pm 1.31	1.86 \pm 0.25	7.4 \pm 0.48	20.32 \pm 1.25	
	Higher 0.75	95.91 \pm 0.14	3.68 \pm 0.19	6.86 \pm 0.21	20.7 \pm 0.88	1.85 \pm 0.17	6.84 \pm 0.22	20.06 \pm 1.12	
	Higher 0.5	95.58 \pm 0.28	4.55 \pm 0.63	7.28 \pm 0.38	20.71 \pm 1.14	1.67 \pm 0.13	7.23 \pm 0.37	19.12 \pm 0.74	
	Higher 0.25	95.98 \pm 0.3	4.28 \pm 0.32	6.66 \pm 0.49	18.73 \pm 0.97	1.24 \pm 0.18	6.65 \pm 0.51	17.06 \pm 0.99	
	Higher 0.1	<u>96.28 \pm 0.03</u>	4.38 \pm 0.16	6.15 \pm 0.05	17.18 \pm 0.28	1.13 \pm 0.11	6.14 \pm 0.04	15.24 \pm 0.37	
	C100	Lower 0.0 / Higher 1.0 (ERM)	73.47 \pm 1.59	13.0 \pm 0.75	39.56 \pm 2.19	121.06 \pm 7.92	2.54 \pm 0.15	36.47 \pm 2.05	100.82 \pm 6.93
		Lower 1.0 / Higher 0.0 (Mixup)	78.11 \pm 0.57	11.92 \pm 0.73	32.82 \pm 0.87	95.76 \pm 2.43	2.49 \pm 0.19	31.06 \pm 0.69	87.94 \pm 1.98
		Lower 0.1	75.40 \pm 0.53	4.72 \pm 0.32	35.87 \pm 0.52	108.38 \pm 1.12	3.48 \pm 0.24	35.92 \pm 0.5	105.87 \pm 1.41
		Lower 0.25	77.14 \pm 0.51	2.56 \pm 0.17	32.93 \pm 0.64	95.47 \pm 1.75	2.54 \pm 0.22	32.95 \pm 0.62	95.42 \pm 1.78
Lower 0.5		77.66 \pm 0.15	3.40 \pm 1.17	32.10 \pm 0.41	90.75 \pm 2.02	1.85 \pm 0.43	31.94 \pm 0.28	89.97 \pm 1.53	
Lower 0.75		78.43 \pm 0.62	4.38 \pm 1.58	30.85 \pm 0.65	86.83 \pm 1.81	1.95 \pm 0.6	30.64 \pm 0.7	85.06 \pm 1.89	
Lower 0.9		79.24 \pm 0.7	6.02 \pm 1.02	<u>30.11 \pm 1.05</u>	85.53 \pm 3.32	1.99 \pm 0.03	<u>29.72 \pm 0.94</u>	82.54 \pm 2.82	
Higher 0.9		77.3 \pm 0.43	3.55 \pm 1.66	32.19 \pm 0.78	90.54 \pm 2.56	<u>1.92 \pm 0.22</u>	32.0 \pm 0.59	88.69 \pm 1.67	
Higher 0.75		77.8 \pm 1.05	3.77 \pm 1.14	31.56 \pm 1.23	90.16 \pm 4.16	2.29 \pm 0.24	31.48 \pm 1.18	88.16 \pm 3.86	
Higher 0.5		78.74 \pm 0.43	4.32 \pm 0.96	30.47 \pm 0.54	86.96 \pm 1.87	2.52 \pm 0.22	30.37 \pm 0.56	84.64 \pm 1.63	
Higher 0.25		78.51 \pm 0.47	3.35 \pm 1.19	30.13 \pm 0.6	85.49 \pm 2.6	2.34 \pm 0.26	30.42 \pm 0.59	84.64 \pm 2.23	
Higher 0.1		<u>79.14 \pm 0.53</u>	5.32 \pm 2.15	29.94 \pm 0.76	85.09 \pm 2.53	2.23 \pm 0.34	29.62 \pm 0.51	82.22 \pm 1.28	

UCE Uncertainty Calibration Error (UCE) (Laves et al., 2020) measures the average of the absolute difference between *mean squared error (MSE)* and *mean variance (MV)* within each bin. It is formally defined by

$$\text{UCE} := \sum_{m=1}^M \frac{|B_m|}{N} |\text{MSE}(B_m) - \text{MV}(B_m)|, \quad (8)$$

with $\text{MSE}(B_m) = \frac{1}{|B_m|} \sum_{i \in B_m} (\mu_{y_i}(\mathbf{x}_i) - y_i)^2$ and $\text{MV}(B_m) = \frac{1}{|B_m|} \sum_{i \in B_m} \sigma_{y_i}^2(\mathbf{x}_i)^2$.

ENCE Expected Normalized Calibration Error (ENCE) (Levi et al., 2022) measures the absolute *normalized* difference, between *root mean squared error (RMSE)* and *root mean variance (RMV)* within each bin. It is formally defined by

$$\text{ENCE} := \frac{1}{M} \sum_{m=1}^M \frac{|\text{RMSE}(B_m) - \text{RMV}(B_m)|}{\text{RMV}(B_m)}, \quad (9)$$

with $\text{RMSE}(B_m) = \sqrt{\frac{1}{|B_m|} \sum_{i \in B_m} (\mu_{y_i}(\mathbf{x}_i) - y_i)^2}$ and $\text{RMV}(B_m) = \sqrt{\frac{1}{|B_m|} \sum_{i \in B_m} \sigma_{y_i}^2(\mathbf{x}_i)^2}$.

D Effect of distance on calibration

In Table 6, we show the exact results for the plot presented in Section 3.1, along with results obtained for different quantiles q . One should compare results of "Lower q " with "Higher $1 - q$ " to have equivalent numbers of possible element to mix with (*diversity*). We repeat our observations here for ease of reading. First, we observe that Mixup improves upon ERM's accuracy, but can degrade calibration depending on the dataset, which is consistent with findings from Wang et al. (2023). Then, when selecting pairs according to distance, a sufficiently high proportion of data to mix is necessary to preserve accuracy ($q > 0.5$). Finally, mixing data with *lower* distances achieves a better calibration as opposed to mixing data with *higher* distances.

E Detailed Algorithm

Algorithm 1 Similarity Kernel Mixup training procedure

Input: Batch of data $\mathcal{B} = \{(\mathbf{x}_i, y_i)\}_{i=1}^n$, similarity parameters $(\tau_{\max}, \tau_{\text{std}})$, model parameters at the current iteration θ_t
 $\tilde{\mathcal{B}} \leftarrow \emptyset$
 $\sigma_t \sim \mathfrak{S}_n$ {Sample random permutation}
for $\forall i \in \{1, \dots, n\}$ **do**
 $\lambda_i \sim \text{Beta}(1, 1)$
 $\tau_i := \tau(\mathbf{x}, i, \sigma; \tau_{\max}, \tau_{\text{std}})$ {Compute warping parameters through Equations (3) and (4)}
 $\tilde{\mathbf{x}}_i := \omega_{\tau_i}(\lambda_i)\mathbf{x}_i + (1 - \omega_{\tau_i}(\lambda_i))\mathbf{x}_{\sigma(i)}$ {Generate new data}
 $\tilde{y}_i := \omega_{\tau_i}(\lambda_i)y_i + (1 - \omega_{\tau_i}(\lambda_i))y_{\sigma(i)}$ {Generate new labels}
 $\tilde{\mathcal{B}} \leftarrow \tilde{\mathcal{B}} \cup (\tilde{\mathbf{x}}_i, \tilde{y}_i)$ {Aggregate new batch}
end for
Compute and optimize loss over $\tilde{\mathcal{B}}$
Output: updated parameters of the model θ_{t+1}

We present a pseudocode of our *Similarity Kernel Mixup* procedure for a single training iteration in Algorithm 1. The generation of new data is explained in the pseudocode as a sequential process for simplicity and ease of understanding, but the actual implementation is optimized to work in parallel on GPU through vectorized operations.

F Proof of Proposition

We give the proof of Proposition 3.1 below:

Proof. Let $\tau > 0$ and $F_\tau(x) = I_x(\tau, \tau)$, then F_τ is the *cumulative distribution function (CDF)* of a Beta distribution with parameters (τ, τ) . $\forall x \in [0, 1]$, we have:

$$P(\omega_\tau(\lambda) \leq x) = P(I_\lambda^{-1}(\tau, \tau) \leq x) \quad (10)$$

$$= P(\lambda \leq I_x(\tau, \tau)) \quad (11)$$

$$= I_x(\tau, \tau), \quad (12)$$

where Equation (11) is obtained since F_τ is continuous and monotonically increasing on $[0, 1]$, and Equation (12) because λ follows a uniform distribution on $[0, 1]$. It follows that $\omega_\tau(\lambda) \sim \text{Beta}(\tau, \tau)$. \square

G Benefits of Warping

G.1 Disentangling Inputs and Targets

Using such warping functions presents the advantage of being able to easily separate the mixing of *inputs* and *targets*, by defining different *warping parameters* $\tau^{(i)}$ and $\tau^{(t)}$:

$$\lambda_t \sim \text{Beta}(1, 1), \quad \begin{aligned} \tilde{\mathbf{x}}_i &:= \omega_{\tau^{(i)}}(\lambda_t)\mathbf{x}_i + (1 - \omega_{\tau^{(i)}}(\lambda_t))\mathbf{x}_{\sigma_t(i)} \\ \tilde{y}_i &:= \omega_{\tau^{(t)}}(\lambda_t)y_i + (1 - \omega_{\tau^{(t)}}(\lambda_t))y_{\sigma_t(i)}. \end{aligned} \quad (13)$$

Disentangling *inputs* and *targets* can be interesting when working in the imbalanced setting (Chou et al., 2020). Notably, with $\tau^{(i)} = 1, \tau^{(t)} \approx 0$, we recover the Mixup Input-Only (IO) variant (Wang et al., 2023) where only inputs are mixed, used in the experiments in Table 1, and with $\tau^{(i)} \approx 0, \tau^{(t)} = 1$, the Mixup Target-Only (TO) variant (Wang et al., 2023), where only labels are mixed. It can also reveal interesting for *structured prediction*, where targets are structured objects such as *graph prediction* or *depth estimation*.

G.2 Computational efficiency

On a more practical side, although the Beta CDF and its inverse have no closed form solutions for non-integer values of its parameters α and β , accurate approximations are implemented in many

Table 7: Comparison of performance (Accuracy in %), calibration (ECE, AECE) after Temperature Scaling, and total training time (in min), with three different variants. All experiments are using a ResNet34 on CIFAR10 on a single A100 GPU and reproduced on 4 different random seeds.

Method	Accuracy (\uparrow)	ECE (\downarrow)	AECE (\downarrow)	Total training time (in min) (\downarrow)
Warping	96.42 \pm 0.24	0.53 \pm 0.06	0.71 \pm 0.05	57.36 \pm 0.31
Warping w/ lookup	96.04 \pm 0.2	0.57 \pm 0.1	0.70 \pm 0.12	55.59 \pm 0.4
No warping	96.3 \pm 0.1	0.55 \pm 0.07	0.76 \pm 0.16	56.88 \pm 1.03

statistical software packages. Then, sampling from Beta distributions with different parameters for each pair of points cannot be done directly on GPU. Coefficients sampled for each pair need to be sent to GPU at each batch, slowing the training because of CPU-GPU synchronizations. An efficient implementation is to define a single `torch.distributions.Beta` with parameters $\alpha = \beta = 1$ (or Uniform) on GPU, and then compute a linear approximation of the inverse Beta CDF from *precomputed lookup tables*, which is common when using inverse transform sampling. We present a comparison in Table 7, in terms of performance (accuracy and calibration) and computation time, of the three different variants of implementation discussed when training a ResNet34 on CIFAR10 on a single A100 GPU ($\tau_{max} = 1, \tau_{std} = 0.4$). The three variants achieve comparable performance, and the time difference is in favour of *using warping functions and lookup tables*.

H Detailed experimental settings

Image Classification For all our experiments, we follow the protocols of Noh et al. (2023). On CIFAR10 and CIFAR100, we use SGD as the optimizer with a momentum of 0.9 and weight decay of 10^{-4} , a batch size of 128, and the standard augmentations `random crop`, `horizontal flip` and `normalization`. Models are trained for 200 epochs, with an initial learning rate of 0.1 divided by a factor 10 after 80 and 120 epochs. On Tiny-ImageNet, models are trained for 100 epochs using SGD with an initial learning rate of 0.1 divided by a factor of 10 after 40 and 60 epochs, a momentum of 0.9 and weight decay of 10^{-4} . We use a batch size of 64 and the same standard augmentations. On Imagenet, models are trained for 100 epochs using SGD with an initial learning rate of 0.1, a cosine annealing scheduler, a momentum of 0.9 and weight decay of 10^{-4} . We use a total batch of 256 split over 3 GPUs and standard augmentations.

Regression Following Yao et al. (2022b), we train a three-layer fully connected network augmented with Dropout Srivastava et al. (2014) on Airfoil, and LST-Attn Lai et al. (2018) on Exchange-Rate and Electricity. All models are trained for 100 epochs with the Adam optimizer Kingma and Ba (2014), with a batch size of 16 and learning rate of 0.01 on Airfoil, and a batch size of 128 and learning rate of 0.001 on Exchange-Rate and Electricity. To estimate variance for calibration, we rely on MC Dropout Gal and Ghahramani (2016) with a dropout of 0.2 and 50 samples.

Method-specific hyperparameters On *classification datasets*, we used $\tau_{max} = 1$ and $\tau_{std} = 0.25$ unless stated otherwise. We used the hyperparameters provided by the authors to reproduce state-of-the-art methods, namely, $\alpha = 1$ and $\Delta\lambda > 0.5$ for MIT-A (Wang et al., 2023), and $w = 0.1$, $\alpha = 2.0$ and $\alpha = 1.0$ for CIFAR10/100 and Tiny-ImageNet respectively, and $Q = 4$, for RankMixup (M-NDCG) (Noh et al., 2023). To compare with Mixup, we use $\alpha = 0.2$, the best performing one found in Thulasidasan et al. (2019), and the same value for Manifold Mixup (Verma et al., 2019). On Imagenet, we set $\tau_{max} = 0.1$ and $\tau_{std} = 0.25$, and $\alpha = 0.1$. On *regression datasets*, we used $(\tau_{max}, \tau_{std}) = (0.0001, 0.5)$ on Airfoil, $(\tau_{max}, \tau_{std}) = (5, 1)$ on Exchange Rate, and $(\tau_{max}, \tau_{std}) = (2, 0.2)$ on Electricity. We followed results from Yao et al. (2022b), and fixed $\alpha = 0.5$ on Airfoil, $\alpha = 1.5$ on Exchange Rate and $\alpha = 2$ on Electricity, for Mixup, Manifold Mixup and C-Mixup. Additionally, we searched for the best *bandwidth* parameter for C-Mixup with cross-validation, and found 0.01 on Airfoil, 0.05 on Exchange Rate, and 0.5 on Electricity. Likewise, we searched for the best α for RegMixup, and found $\alpha = 0.5$ on Airfoil, $\alpha = 10$ on Exchange-Rate and $\alpha = 10$ on Electricity.

Table 8: Comparison of Accuracy and ECE, before and after Temperature Scaling (TS), with cross-validation when varying τ_{std} . Results are obtained with a Resnet50 and averaged over 4 splits.

Dataset	τ_{std}	Accuracy	ECE (\downarrow)	TS ECE (\downarrow)
CIFAR10	0.25	95.18	2.87	0.97
	0.4	95.23	3.31	1.42
	0.5	95.37	2.7	2.08
	0.6	95.45	3.15	1.99
	0.75	95.57	3.44	2.05
	0.8	95.44	3.28	2.07
	1	95.57	3.44	2.05
	1.25	95.46	2.71	2.25
	1.5	95.29	3.42	2.36
	2	94.93	3.24	2.43
CIFAR100	0.25	77.74	3.98	1.77
	0.4	78.26	4.24	2.4
	0.5	78.37	3.45	3.61
	0.6	78.29	2.9	4.08
	0.75	78	3.65	3.91
	0.8	78.03	3.33	4.27
	1	77.35	4.82	3.4
	1.25	77.31	3.98	3.88
	1.5	77.92	4.19	4.06

I On the selection and sensitivity to hyperparameters

As discussed in Section 3.2, we always draw initial interpolation parameters λ from Beta(1,1), removing α as a hyperparameter. Then, τ_{max} and τ_{std} can be tuned separately, and, as mentioned in Section 4.2, we found that impact on calibration was mainly controlled by τ_{std} . We selected the values giving the best trade-off between accuracy and calibration using cross-validation, with a stratified sampling on a 90/10 split of the training set, similarly to Pinto et al. (2022), and average the results across 4 different splits. We detail in Table 8 cross-validation results (Accuracy and ECE) showing sensitivity to τ_{std} on CIFAR10 and CIFAR100 datasets, using a ResNet50. These results lead us to using $\tau_{std} = 0.25$ for all image classification experiments, and show that our approach is not that sensitive to hyperparameter choice between datasets. For Imagenet, we set $\tau_{max} = 0.1$ to follow the commonly used value of $\alpha = 0.1$ in Mixup for this dataset.

J On the choice of similarity kernel

J.1 On Warping functions

As discussed in Section 3.3, the choice of the similarity kernel is highly dependent on the warping function, and more specifically to the correlation between the warping parameter and the shape of the warping function. Given our choice of using the inverse of the Beta CDF as ω_τ , and that its shape is logarithmically correlated to τ , the choice of a Gaussian kernel seems natural to have an exponential correlation with the distance. Then, the normalization and centering avoid dealing with different range of embedding values between datasets and architectures when choosing a correct value of τ_{std} . Regarding the choice of warping function, as mentioned in Section 3.2, any bijection with a sigmoidal shape could be considered. Besides the inverse of Beta CDF, we also tried the Beta CDF and the Sigmoid ($\lambda \mapsto \frac{1}{1+e^{\lambda/\tau}}$). As they all have logarithmic correlations wrt τ , we used our Gaussian similarity kernel for the three of them. We compare performance on Airfoil dataset after finding the best parameters in each case in Table 9. The inverse of Beta CDF have both the advantage of better results, while preserving the underlying Beta distribution by inverse transform sampling, as we show in Proposition 3.1.

Table 9: Performance (RMSE, MAPE) and calibration (UCE, ENCE) comparison for different warping functions on Airfoil dataset. Averaged over 10 random seeds.

Warping	RMSE (\downarrow)	MAPE (\downarrow)	UCE (\downarrow)	ENCE (\downarrow)
Sigmoid	2.892 ± 0.343	1.733 ± 0.229	117.95 ± 45.26	0.018 ± 0.008
Beta CDF	2.807 ± 0.261	1.694 ± 0.176	126.02 ± 23.32	0.018 ± 0.005
Inverse Beta CDF	2.707 ± 0.199	1.609 ± 0.137	93.79 ± 25.46	0.019 ± 0.008

Table 10: Performance (RMSE, MAPE) and calibration (UCE, ENCE) comparison for different similarity distance on Airfoil dataset. Averaged over 10 random seeds.

Warping	RMSE (\downarrow)	MAPE (\downarrow)	UCE (\downarrow)	ENCE (\downarrow)
Input distance	2.848 ± 0.355	1.706 ± 0.215	105.23 ± 26.32	0.018 ± 0.008
Embedding distance	2.737 ± 0.205	1.636 ± 0.142	101.62 ± 21.94	0.016 ± 0.005
Label distance	2.707 ± 0.199	1.609 ± 0.137	93.79 ± 25.46	0.019 ± 0.008

J.2 On embedding spaces and distances

J.2.1 Regression tasks

As discussed in Section 3.3, in regression tasks, we considered either input, embedding or label distance:

- **Input distance:** $\bar{d}_n(\mathbf{x}_i, \mathbf{x}_{\sigma(i)})$,
- **Embedding distance:** $\bar{d}_n(h_\varphi(\mathbf{x}_i), h_\varphi(\mathbf{x}_{\sigma(i)}))$,
- **Label distance:** $\bar{d}_n(y_i, y_{\sigma(i)})$.

Input and label distances both have the advantages of inducing almost no computational overhead, as opposed to embedding distance that requires an additional forward pass in the network. We report results comparing the three options on Airfoil dataset in Table 10. We found that label distance was the best performing one, which is in line with results from Yao et al. (2022b), and what we use in the experiments in Section 4.3.

J.2.2 Classification tasks

In classification tasks, as we lack a meaningful distance between label, we restricted our choice between input and embedding distance. Even though computing distances directly in the input space is faster than relying on embeddings, the latter achieves a better trade-off between accuracy and calibration improvements, which motivated us to use embedding distances as similarity in our experiments in Section 4.2. We compare in Table 11 the two distances, for the different value of τ_{std} , using a Resnet34 on CIFAR10 and CIFAR100 datasets.

Table 11: Comparison of performance (Accuracy in %), calibration (ECE) after Temperature Scaling, for two different similarity distance. All experiments are using a ResNet34 on CIFAR10 and CIFAR100 datasets and averaged over 4 different random seeds.

Dataset	Distance	τ_{std}	Accuracy (\uparrow)	ECE (\downarrow)
CIFAR10	Input distance	0.2	95.82 \pm 0.19	0.41 \pm 0.13
		0.4	96.10 \pm 0.17	0.46 \pm 0.06
		0.6	95.87 \pm 0.47	0.6 \pm 0.13
		0.8	96.12 \pm 0.15	0.70 \pm 0.08
		1.0	96.01 \pm 0.27	0.74 \pm 0.19
	Embedding distance	0.2	96.29 \pm 0.07	1.35 \pm 0.14
		0.4	96.42 \pm 0.24	0.53 \pm 0.06
		0.6	96.36 \pm 0.09	0.52 \pm 0.08
		0.8	96.0 \pm 0.41	0.56 \pm 0.05
		1.0	96.25 \pm 0.07	0.55 \pm 0.12
CIFAR100	Input distance	0.2	78.43 \pm 0.52	1.51 \pm 0.10
		0.4	78.24 \pm 0.35	1.35 \pm 0.22
		0.6	78.36 \pm 0.97	1.5 \pm 0.20
		0.8	78.50 \pm 0.41	1.5 \pm 0.16
		1.0	78.50 \pm 0.83	1.53 \pm 0.08
	Embedding distance	0.2	78.13 \pm 0.52	1.31 \pm 0.23
		0.4	78.86 \pm 0.83	1.42 \pm 0.19
		0.6	78.63 \pm 0.27	1.74 \pm 0.30
		0.8	79.12 \pm 0.52	1.66 \pm 0.16
		1.0	78.51 \pm 0.94	1.49 \pm 0.03